Title

Computational cell analysis for label-free detection of cell properties in a microfluidic laminar flow

Journal

Analyst, 141(13)

ISSN

0003-2654

Authors

Zhang, Alex Ce
Gu, Yi
Han, Yuanyuan
et al.

Publication Date

2016-06-20

DOI

10.1039/c6an00295a

Peer reviewed

Published in final edited form as:

Analyst. 2016 June 20; 141(13): 4142–4150. doi:10.1039/c6an00295a.

Computational cell analysis for label-free detection of cell properties in a microfluidic laminar flow

Alex Ce Zhang[a,†], **Yi Gu**[a,†], **Yuanyuan Han**[a], **Zhe Mei**[b], **Yu-Jui Chiu**[c], **Lina Geng**[d], **Sung Hwan Cho**[b], and **Yu-Hwa Lo**[a,c,*]

[a]Department of Electrical and Computer Engineering, University of California at San Diego, La Jolla, California 92093-0407, USA

[b]Nanocellect Biomedical, Inc, San Diego, CA 92121

[c]Materials Science and Engineering Program, University of California, San Diego, 9500 Gilman Drive, La Jolla, California 92093-0418, USA

[d]School of life sciences, Beijing Institute of technology, Beijing 100081, China

Abstract

Although flow cytometer, being one of the most popular research and clinical tools for biomedicine, can analyze cells based on cell size, internal structures such as granularity, and molecular markers, it provides little information about the physical properties of cells such as cell stiffness and physical interactions between cell membrane and fluid. In this paper, we propose a computational cell analysis technique using cells' different equilibrium positions in a laminar flow. This method utilizes a spatial coding technique to acquire the spatial position of the cell in a microfluidic channel and then uses mathematical algorithms to calculate the ratio of cell mixtures. Most uniquely the invented computational cell analysis technique can unequivocally detect the subpopulation of each cell type without labeling even when the cell type shows a substantial overlap in the distribution plot with other cell types, a scenario limiting the use of conventional flow cytometers and machine learning techniques. To prove this concept, we have applied the computation method to distinguish live and fixed cancer cells without labeling, count neutrophil from human blood, and distinguish drug treated cells from untreated cells. Our work paves the way for using computation algorithms and fluidic dynamic properties for cell classification, a label-free method that can potentially classify over 200 types of human cells. Being a highly cost-effective cell analysis method complementary to flow cytometers, our method can offer orthogonal tests in companion with flow cytometers to provide crucial information for biomedical samples.

Introduction

For decades, flow cytometers have been used to measure physical properties of cells such as their size and granularity [1–7]. Although labelling allows further differentiation of cells from fluorescent signals [7–13], cell labelling could unintentionally modify the property of cells [8] and in some cases affect cell viability [14–15] in addition to adding cost and

*Corresponding author: ylo@ucsd.edu.
†These authors contributed equally to this work.

process complexity. Therefore, significant efforts have been devoted to attaining as much cell information as possible without labelling [16–21]. In this paper we demonstrated enhanced abilities of label-free detection and analysis of cells in a laminar flow by employing innovative computation algorithms. Indeed, there have been numerous successful examples [22–23] for applications of computation algorithms to obtain extra cellular information from biological samples, as demonstrated in super-resolution microscopy [24–28] and imaging flow cytometer [29].

Realizing that cells of different physical properties find different equilibrium positions in a microfluidic laminar flow [30–39], we can acquire valuable cellular information from cell positions in principle. However, up to now such information has not become much useful because different types of cells or the same type of cells in different conditions (e.g. drug treatments or infections) often produce very small position differences in a fluidic channel. To overcome this problem, at first we have to find a scheme to detect very small (a fraction of cell size) positional changes. A few years ago, we invented a space-time coding method to detect the cell position with better than one micrometer resolution [40–45]. However, we still face another challenging problem resulted from the intrinsic inhomogeneity of biological cells. In other words, the property variations within the same cell group can be comparable to or even greater than the variations between two different cell groups. As a result, the distribution plots of two different cell groups may seriously overlap that no machine learning methods such as support vector machine (SVM) algorithms are able to separate the two groups [41]. The key contribution of this paper is to devise an entirely new concept to address this critical issue. Instead of trying to classify each individual cells, we detect cells and their properties by groups. For two or more groups of cells with slightly different properties, our computation algorithms can (a) determine the cell population of each group, and (b) determine the spread and inhomogeneity of the properties within each cell group. Using the proposed computation method, we have demonstrated that even though the two cell groups have their distribution plots overlapped by 80% or more, one can still accurately measure the population of each group of cells in samples of cell mixture. To showcase potential applications of the computational cell analysis method, we demonstrate such unique capabilities in two examples. For point of care, we count neutrophil in whole blood for neutropenia detection, a critical and frequent test for chemotherapy patients [46–51]. For drug testing based on phenotypical properties, we detect cellular response to drugs for target proteins (e.g. G-protein-coupled receptors) [52–53].

Experimental Method

Computational cell analysis technique

1. Measurement of cell position within a microfluidic channel—In a microfluidic channel, cells of different physical properties (size, shape, stiffness, morphology, etc.) experience different magnitudes of lift and drag force, thus yielding different equilibrium positions in the laminar flow [30–39].

To determine the equilibrium position of a particular cell in the microfluidic channel, a spatial coding method was used to obtain the horizontal position and the velocity of the cell. The design and configuration of the system is illustrated in figure 1. The spatial mask has

two oppositely oriented trapezoidal slits with the base lengths being 100 *um* and 50 *um* (figure 2(a)). An LED source was used to illuminate from the bottom of the microfluidic channel. The transmitted signal was detected by a variable gain photoreceiver made of a Si photodiode and a transimpedance amplifier (Thorlab). All light blocking areas on the spatial mask was coated with a layer of Ti/Au on a glass slide. When cells flew through the spatial mask area, their forward scattering signal gave rise to a characteristic waveform encoded by the mask. The microfluidic channel is 5 *cm* long and has its inlet and outlet at the ends. The rectangular cross section of the channel is 100 *um* wide and 50 *um* high. The mask is located at 4.5 *cm* from the inlet. In the following discussion, we will represent the channel width direction as x-axis and channel height direction as y-axis. The intensity modulated FS signal by the trapezoidal slits displays 2 peaks, as shown in figure 2(b). The ratio between the width of the first peak and the second peak provides information of the cell position in the X-axis; and the absolute value of the signal width gives information about cell velocity. Knowing the position along the x-axis and the cell velocity, the cell position along the y-axis can be obtained using the property of laminar flow that gives rise to a parabolic velocity profile represented by the following relation [39–44]:

$$y = h \times \sqrt{1 - \frac{V(x,y)}{V_{\max} \times \left[1 - \left(\frac{x - L/2}{L/2}\right)^2\right]}}$$

In the above equation, y is the cell position in the channel height direction (y-axis), h is the half channel height, 25 μ*m* in this work. x is the horizontal position. $V(x, y)$ is the velocity at a specific position. L is the channel width in the horizontal direction, in our case 100 μ*m*. V_{max} is the maximum velocity occurring at the center of the channel (i.e. $x = L/2$, $y = 0$, in our case, $x = 50$ μ*m*, $y = 0$ μ*m*). The target cells are suspended in PSB buffer solution ($\rho = 10^3 kg \cdot m^{-3}$, $\mu = 1.05 \times 10^{-3} Pa \cdot s$) The flow rate used in the experiment is 180 μ*L/min*. The microchannel hydraulic diameter, $D_h = (2W \times h)/(W + H)$, is 66.7 μ*m*, where W and H are the width and height of the channel. The Reynolds number is calculated to be 38.1.

2. Computational cell analysis methods

Basic algorithms: For a given type of cells in a channel, their equilibrium positions can be represented by a characteristic distribution $R(x, y)$. The characteristic distribution can be obtained in a diluted sample to avoid any effects caused by cell-cell interactions in the flow. Figure 3 shows the characteristic distribution of live MDA-MB-231 cells. Without cell-cell interactions in the fluid, the spatial distribution of a sample containing multiple cell groups is the linear combination of the characteristic functions of each cell type.

If $R_A(x, y)$ and $R_B(x, y)$ are the characteristic functions of cell type A and cell type B, the spatial distribution, $S(x, y)$, for a mixture of cell A and cell B can be described by Eq. (1) where the coefficient, C, is the fraction of cell A in the sample.

$$S(x,y) = C \times R_A(x,y) + (1 - C) \times R_B(x,y) \quad (1)$$

Since both $R_A(x, y)$ and $R_B(x, y)$ are normalized over the entire cross section of the fluidic channel,

$$\iint_{x,y} R_A(x,y)dxdy=1 \text{ and } \iint_{x,y} R_B(x,y)dxdy=1$$

The distribution function $S(x, y)$ for the sample is also normalized as in (2).

$$\iint_{x,y} S(x,y)dxdy=C\times\iint_{x,y} R_A(x,y)dxdy+(1-C)\times \iint_{x,y} R_B(x,y)dxdy=1 \quad (2)$$

If we already know $R_A(x, y)$, $R_B(x, y)$ from the training data and measure $S(x, y)$ from the sample, we can find from Eq. 1 the only unknown, C, being the population of cell A, which is the information of interest.

In practice, the values of $R_A(x, y)$, $R_B(x, y)$, *and* $S(x, y)$ at each specific position (x, y) are random variables. We divide the whole area of the channel cross section into meshes so the sets of random variables $R_A(x, y)$, $R_B(x, y)$, *and* $S(x, y)$ follow the relations:

$$\sum_{x,y} R_A(x,y)=1 \text{ and } \sum_{x,y} R_B(x,y)=1$$

$$\sum_{x,y} S(x,y)=C\times\sum_{x,y} R_A(x,y)+(1-C)\times\sum_{x,y} R_B(x,y)=1 \quad (3)$$

Due to the statistical nature of the problem, the resulting value of C, calculated at each position (x, y), is also a random variable. Thus we can plot the distribution of C, the percentage of cell A in the sample, in a histogram. The mean value of the histogram produces the most likely percentage for cell A in the sample and the spread of the histogram provides a good indication of the quality of the measurement. Figure 5 shows an example of the histogram for C.

Therefore, for any cell type possessing even a slightly different physical property than the rest of the cells in the sample, manifested by its largely overlapped spatial distribution with the rest of the samples, our method is still able to find the relative population of such specific cell type in a cell mixture. This is a unique capability of the proposed method.

Obtaining characteristic functions from practical, non-purified, samples

In some practical cases, pure samples of a single cell type are not always available to allow us to obtain the characteristic functions (e.g. $R_A(x, y)$, $R_B(x, y)$, *etc.*). Even in the cases where one can use cultured cells to produce samples of pure cells, the distributions obtained from the cultured cells may be different from the real cells of the same type in physiological conditions.

In the following we describe how one can obtain the characteristic functions (i.e. $R_A(x, y)$, $R_B(x, y)$, *etc.*) from cell mixtures directly without pure samples. These cell mixtures can come directly from patient samples. To elucidate this method, let us start with two (or more) samples with different ratios (i.e. C_1 and C_2) of mixture between cell A and cell B. We obtain the following relations:

$$S_1(x,y)=C_1R_A(x,y)+(1-C_1)R_B(x,y)$$

$$S_2(x,y)=C_2R_A(x,y)+(1-C_2)R_B(x,y) \quad (4)$$

For training samples, we can label cells A and B so that one can use a conventional flow cytometer to find the cell ratios, C_1 and C_2 of the two training samples. The left hand side (LHS) of Eq. (4) are the measured distribution functions for the two mixtures. Then at each position (x, y), we can use Eq. (4) to find the characteristic functions $R_A(x, y)$ and $R_B(x, y)$ for cells A and B since C_1 and C_2 are already known. Note that we only need to perform the above experiment once to establish the "library" of the characteristic functions for all cells of interest, and then these characteristic functions can be used for all future analysis of samples consisting of various cell mixtures. This process is further illustrated in figure 6.

For a mixture of two cell types with an unknown mixing ratio (C_3), we can find its value using the same method described above (figure 7).

Note that the distribution function $R(x, y)$ for each sample represents a set of position dependent random variables, so the reliability of its value at each position depends on the size of the ensemble within each mesh. To assure a good ensemble size at each position and to obtain the highest possible spatial resolution for $R(x, y)$, we design meshes using the quad-tree algorithm that balances the weight of each mesh and the spatial resolution to yield the most distinctive and statistically sound results for cell detection.

Mesh definition for distribution functions: the quad-tree algorithm

Since the spatial distribution of the cell is not uniform across the channel, the weight of each mesh will be inevitably biased if the channel is divided up into meshes of uniform size. In such case, the information contained in those meshes with few cells flowing through (i.e. fewer data points) is less reliable. Those meshes, which may represent the majority of meshes for a distribution function concentrated to a relatively small area, can produce large noise and degrade the accuracy and confidence level of the result. On the other hand, for those meshes where there are too many cells flowing through, we do not take full advantage of the spatial resolution the data offer. To address these issues, we adopt meshes with non-uniform size based on the quad-tree algorithm [53]. The quad-tree algorithm chooses mesh sizes dynamically based on the density of recorded cell positions. The channel is first divided into 4 meshes, each of which is further divided into another 4 meshes. Such process continues to form a quad tree. Then the number of cells travelling through each mesh in each generation of quad in the tree is counted. If the number of cells within an older generation of

quad (i.e. larger sized quad) is greater than the threshold for a statistically reliable ensemble, the next generation of quad will be used to gain a higher spatial resolution with a reduced ensemble size. The process continues until the smallest quads with slightly above threshold cell counts are reached. Figure 8 shows how meshes are determined for a spatial distribution using the quad-tree algorithm. In this example, the distribution function was obtained by flowing 10,000 cells through a 100 $\mu m \times 50\ \mu m$ channel.

Experimental results

Detection of the population of live and fixed cells

Without labelling, today's flow cytometers cannot find the percentage of live and dead cells in a culture because the scattering signals (forward, side, and back scattering) between live and dead cells overlap significantly in the distribution plot. We demonstrate that in spite of the high similarity in their physical properties of live and dead cells, the computation cell analysis technique enables us to give an unequivocal answer to the subpopulation of live cells from dead cells.

We used live and fixed MDA-MB-231 cells to demonstrate the concept. MDA-MB-231 is a cell line for human breast cancer. In the experiment, we fixed one group of cultured MDA-MB-231 cells and labelled them fluorescently (Propidium Iodide), and then mixed these fixed cells with live cells in different ratios. Each sample with a specific ratio of live and fixed cells was divided into two parts, one running through our device and the other running through a commercial flow cytometer. Figure 9(a) shows the distribution plot for forward and side scattering signals from a flow cytometer. It was impossible to determine the ratio between live and fixed MDA-MB-231 cells from the scattering signals by any gating or machine learning algorithms due to the significant overlap of the signals from live and dead cells. The only reliable method for a flow cytometer to detect the relative population of live cells from dead cells is by fluorescent labelling as shown in Figure 9(b). Next we demonstrate how the computation cell analysis method can solve this problem.

To produce characteristic functions for live and dead MDA-MB-231 cells, we ran through our system with two samples with 100% live MDA-MB-231 and 100% fixed MDA-MB-231. Figure 10 shows the characteristic functions of live MDA-MB-231 cells and fixed MDA-MB-231 cells over the proposed quad-tree meshes. Figure 11 shows the characteristic functions in a way that each mesh was assigned an index according to the ascending value of the characteristic function. Figure 11 clearly reveals the differences in the characteristic function between live and fixed MDA-MB-231 cells. Then we ran multiple test samples with different ratios of live and fixed MDA-MB-231 cells. For each test sample, we ran the experiment 10 times, taking 3 minutes for each run, to test the reproducibility and reliability of the results. Figure 12 shows comparisons between our method and the flow cytometer results by detecting the fluorescent signals of fluorescently labelled fixed cells. The excellent agreement and similar repeatability (10 repeats) of the results from both methods demonstrate the accuracy and reliability of our label-free computation cell analysis method.

Neutrophil counter for point-of-care applications

There are three major types of white blood cells, neutrophil, lymphocyte, and monocyte. Neutrophil count is an indicator of patient's immunity to infections and is particularly important for cancer patients undergoing chemotherapy since the treatment can lower neutrophil count. Neutropenia develops when the neutrophil count falls below certain levels, substantially increasing the risk of infections [46⁻47]. Therefore, the neutrophil count of chemotherapy patients has to be closely monitored, presenting the need for point-of-care neutrophil counter without fluorescent labelling. In the following we demonstrate how the computation cell analysis technique can count neutrophil in a point-of-care setting.

We performed the experiment using purchased blood from San Diego blood bank. After red blood cell lysing, the blood was diluted with 1× PBS solution. Since we were interested in neutrophil count, we treated neutrophil as cell A and all non-neutrophil WBCs as cell B. Then we represent the characteristic function for neutrophil as $R_A(x, y)$ and all non-neutrophil white blood cells (WBCs) as $R_B(x, y)$. To obtain $R_A(x, y)$ and $R_B(x, y)$, we did not use blood samples with 100% pure neutrophils since complete removal of neutrophil from the samples can be practically difficult. Instead, we chose two blood samples with different neutrophil to non-neutrophil ratios. We used superparamagnetic beads (Dynabeads from ThermoFisher) to remove some neutrophils from the blood to produce samples with lower than normal amounts of neutrophil, which also simulated neutropenia patients. Using the aforementioned protocol, the superparamagnetic beads--Dynabeads CD15--that were covalently coupled with an anti-human CD15 antibody were used to deplete human CD15+ myeloid cells, predominantly neutrophils, directly from whole blood. Different concentrations of Dynabeads CD15 were used to create blood samples having various percentages of neutrophil [55].

Using the above mentioned algorithm (see Fig. 6), we obtained the characteristic functions of neutrophil and non-neutrophil as shown in Figure 13. From these characteristic functions, one could apply Eq. (4) to find the neutrophil ratio from samples of an unknown neutrophil population. Again, we have divided each test sample into two parts, one going through our device and another going through a commercial flow cytometer (Accuri C6). For each sample the test was repeated 10 times. Figure 14 shows the comparison of results from both methods. The experiment was designed to cover the whole range of neutrophil ratio to simulate healthy samples and samples with different degrees of neutropenia.

Table 1 summarizes results from another set of experiment out of 8 purchased blood samples from San Diego blood bank. The excellent agreement between the proposed method and the commercial flow cytometer shows that the computational cell analysis device, being a highly flexible and versatile technique, can operate as a cost effective, point-of-care neutrophil counter.

Drug response test from cell's phenotypical characteristics

The computational cell analysis technique is capable of capturing minor changes in cell properties (e.g. cell size, shape, granularity, stiffness, surface properties, etc.) that are often hard to detect under conventional histology analysis. The unique ability of detecting such

otherwise hard-to-detect cell property changes provides valuable insight and complements the existing methods in drug discovery. Drug responses of cells, especially the early stage response or responses under low drug dosage, may not be obvious and can skip people's attention [9]. We have performed preliminary studies to investigate our method's capability of detecting subtle changes of cell properties under drug treatments.

We divided breast cancer cells (MDA-MB-231) into two groups. For the first group, 15nM of Paclitaxel was introduced to around one million cells for 48 hours. As a cytoskeletal drug, Paclitaxel stabilizes the microtubule cytoskeleton against depolymerization [56], and is reported to affect cell surface roughness and stiffness [57] due to increase in microtubule rigidity [56]. As a control group, we introduced no drug to the second group of cells that were also cultured for 48 hours. Then the two groups of cells were run through our computation cell analysis system, yielding two characteristic functions corresponding to the drug treated and untreated cells. In figure 15, the X-axis is the index of the meshes following the quad-tree algorithm (see Figure 8), and the Y-axis is the value of characteristic function. The difference of the characteristic function between the drug treated and untreated cells was presented in figure 15 where each mesh was assigned an index according to the ascending value of the characteristic function. Such representation helps us visualize and quantify the differences of characteristic functions between cells. From figure 15 we observed clear differences between MDA-MB-231 cells with and without Paclitaxel treatment, suggesting the fluid mechanic properties of the cells have been affected by the drug although the alterations of cell's phenotypical features were not apparent under fluorescent microscope (figure 16).

Conclusions

In this paper, we report the invention of computational cell analysis as an entirely new method of detecting and analyzing cells from their spatial distribution in the microfluidic channel. A spatially coded mask was used to obtain the position of each cell by its optical scattering center. A mathematical algorithm was developed to calculate the composition of the cell mixture in the sample. This method is inherently label free and provides unique cellular information complementary to existing flow cytometers. Because the information is extracted from computation algorithms, the hardware of the apparatus is simple and inexpensive, making it suitable for point-of-care applications and amendable to many biomedical applications. To show the versatility of the technique, in this paper we demonstrate the functions of counting the population of live and dead cells, counting neutrophils from whole blood for neutropenia detection, and detecting cell property changes under drug treatments. These are a few examples from a large number of possible applications of the technique. We believe the method of computational cell analysis opens a new avenue for cell analysis and offers a myriad of opportunities and capabilities complementary to the existing methods.

Acknowledgments

The authors acknowledge the technical support of the staff of the San Diego Nanotechnology Infrastructure (SDNI), which is part of the National Nanotechnology Coordinated Infrastructure (NNCI). Research reported in this publication was supported by the National Institute of General Medical Sciences of the National Institutes of Health

under Award Number R43GM109241. The content is solely the responsibility of the authors and does not necessarily represent the official views of the National Institutes of Health.

References

1. Godin, Jessica, et al. Microfluidics and photonics for Bio-System-on-a-Chip: A review of advancements in technology towards a microfluidic flow cytometry chip. Journal of biophotonics. 2008; 1.5:355. [PubMed: 19343660]
2. Pang, Lin, et al. Optofluidic devices and applications in photonics, sensing and imaging. Lab on a Chip. 2012; 12.19:3543–3551. [PubMed: 22810383]
3. Piorek, Brian D., et al. Free-surface microfluidic control of surface-enhanced Raman spectroscopy for the optimized detection of airborne molecules. Proceedings of the National Academy of Sciences. 2007; 104.48:18898–18901.
4. Wu, Jigang; Zheng, Guoan; Lee, Lap Man. Optical imaging techniques in microfluidics and their applications. Lab on a Chip. 2012; 12.19:3566–3575. [PubMed: 22878811]
5. Monat C, Domachuk P, Eggleton BJ. Integrated optofluidics: A new river of light. Nature photonics. 2007; 1.2:106–114.
6. Godin, Jessica, et al. Microfluidics and photonics for Bio-System-on-a-Chip: A review of advancements in technology towards a microfluidic flow cytometry chip. Journal of biophotonics. 2008; 1.5:355. [PubMed: 19343660]
7. Vezenov, Dmitri V., et al. Integrated fluorescent light source for optofluidic applications. Applied Physics Letters. 2005; 86.4:41104–41104.
8. Brown, Michael; Wittwer, Carl. Flow cytometry: principles and clinical applications in hematology. Clinical chemistry. 2000; 46.8:1221–1229. [PubMed: 10926916]
9. Xi, Biao, et al. The application of cell-based label-free technology in drug discovery. Biotechnology journal. 2008; 3.4:484–495. [PubMed: 18412175]
10. Chin, Curtis D.; Linder, Vincent; Sia, Samuel K. Lab-on-a-chip devices for global health: Past studies and future opportunities. Lab on a Chip. 2007; 7.1:41–57. [PubMed: 17180204]
11. Whitesides, George M. The origins and the future of microfluidics. Nature. 2006; 442.7101:368–373. [PubMed: 16871203]
12. Cho, Sung Hwan, et al. Review article: recent advancements in optofluidic flow cytometer. Biomicrofluidics. 2010; 4.4:043001.
13. Chin, Curtis D., et al. Microfluidics-based diagnostics of infectious diseases in the developing world. Nature medicine. 2011; 17.8:1015–1019.
14. Fu, Yingli; Kraitchman, Dara L. Stem cell labeling for noninvasive delivery and tracking in cardiovascular regenerative therapy. 2010:1149–1160.
15. Gholamrezanezhad, Ali, et al. Cytotoxicity of 111In-oxine on mesenchymal stem cells: a time-dependent adverse effect. Nuclear medicine communications. 2009; 30.3:210–216. [PubMed: 19262283]
16. Gossett, Daniel R., et al. Label-free cell separation and sorting in microfluidic systems. Analytical and bioanalytical chemistry. 2010; 397.8:3249–3267. [PubMed: 20419490]
17. Cheng, Xuanhong, et al. A microfluidic device for practical label-free CD4+ T cell counting of HIV-infected subjects. Lab on a Chip. 2007; 7.2:170–178. [PubMed: 17268618]
18. Blasi, Thomas, et al. Label-free cell cycle analysis for high-throughput imaging flow cytometry. Nature communications. 2016; 7
19. Shan, Xiaonan; Foley, Kyle J.; Tao, Nongjian. A label-free optical detection method for biosensors and microfluidics. Applied Physics Letters. 2008; 92.13:133901.
20. Vollmer, Frank; Arnold, Stephen. Whispering-gallery-mode biosensing: label-free detection down to single molecules. Nature methods. 2008; 5.7:591–596. [PubMed: 18587317]
21. Cheung, Karen; Gawad, Shady; Renaud, Philippe. Impedance spectroscopy flow cytometry: on-chip label-free cell differentiation. Cytometry Part A. 2005; 65.2:124–132.

22. Morrill, Gene A.; Kostellow, Adele B.; Gupta, Raj K. Computational analysis of the extracellular domain of the Ca 2+-sensing receptor: An alternate model for the Ca 2+ sensing region. Biochemical and biophysical research communications. 2015; 459.1:36–41. [PubMed: 25701780]
23. Rooney, Katherine E. Computational modeling of extracellular dopamine kinetics suggests low probability of neurotransmitter release. Synapse. 2015; 69.11:515–525. [PubMed: 26248886]
24. Shtengel, Gleb, et al. Interferometric fluorescent super-resolution microscopy resolves 3D cellular ultrastructure. Proceedings of the National Academy of Sciences. 2009; 106.9:3125–3130.
25. Mortensen, Kim I., et al. Optimized localization analysis for single-molecule tracking and super-resolution microscopy. nature methods. 2010; 7.5:377–381. [PubMed: 20364147]
26. Holden, Seamus J.; Uphoff, Stephan; Kapanidis, Achillefs N. DAOSTORM: an algorithm for high-density super-resolution microscopy. Nature methods. 2011; 8.4:279–280. [PubMed: 21451515]
27. Huang, Bo, et al. Three-dimensional super-resolution imaging by stochastic optical reconstruction microscopy. Science. 2008; 319.5864:810–813. [PubMed: 18174397]
28. Huang, Bo; Bates, Mark; Zhuang, Xiaowei. Super resolution fluorescence microscopy. Annual review of biochemistry. 2009; 78:993.
29. Han, Yuanyuan; Lo, Yu-Hwa. Imaging Cells in Flow Cytometer Using Spatial-Temporal Transformation. Scientific reports. 2015; 5
30. Di Carlo, Dino, et al. Continuous inertial focusing, ordering, and separation of particles in microchannels. Proceedings of the National Academy of Sciences. 2007; 104.48:18892–18897.
31. Di Carlo, Dino, et al. Equilibrium separation and filtration of particles using differential inertial focusing. Analytical chemistry. 2008; 80.6:2204–2211. [PubMed: 18275222]
32. Oakey, John, et al. Particle focusing in staged inertial microfluidic devices for flow cytometry. Analytical chemistry. 2010; 82.9:3862–3867. [PubMed: 20373755]
33. Bhagat, Ali Asgar S.; Kuntaegowdanahalli, Sathyakumar S.; Papautsky, Ian. Enhanced particle filtration in straight microchannels using shear-modulated inertial migration. Physics of Fluids (1994-present). 2008; 20.10:101702.
34. Yun, Hoyoung, et al. Simultaneous counting of two subsets of leukocytes using fluorescent silica nanoparticles in a sheathless microchip flow cytometer. Lab on a Chip. 2010; 10.23:3243–3254. [PubMed: 20941407]
35. Hur, Soojung Claire; Tse, Henry Tat Kwong. Sheathless inertial cell ordering for extreme throughput flow cytometry. Lab on a Chip. 2010; 10.3:274–280. [PubMed: 20090998]
36. Hur, Soojung Claire, et al. Deformability-based cell classification and enrichment using inertial microfluidics. Lab on a Chip. 2011; 11.5:912–920. [PubMed: 21271000]
37. Mortazavi, Saeed; Tryggvason, Grétar. A numerical study of the motion of drops in Poiseuille flow. Part 1. Lateral migration of one drop. Journal of Fluid Mechanics. 2000; 411:325–350.
38. Pamme, Nicole. Continuous flow separations in microfluidic devices. Lab on a Chip. 2007; 7.12:1644–1659. [PubMed: 18030382]
39. Godin, Jessica; Lien, Victor; Lo, Yu-Hwa. Demonstration of two-dimensional fluidic lens for integration into microfluidic flow cytometers. Applied Physics Letters. 2006; 89.6:061106.
40. Wu, Tsung-Feng; Mei, Zhe; Lo, Yu-Hwa. Optofluidic device for label-free cell classification from whole blood. Lab on a Chip. 2012; 12.19:3791–3797. [PubMed: 22875178]
41. Wu, Tsung-Feng; Mei, Zhe; Lo, Yu-Hwa. Label-free optofluidic cell classifier utilizing support vector machines. Sensors and Actuators B: Chemical. 2013; 186:327–332.
42. Wu, Tsung-Feng, et al. SPIE MOEMS-MEMS. International Society for Optics and Photonics; 2013. Rapid white blood cell detection for peritonitis diagnosis.
43. Wu, Tsung-Feng, et al. Handbook of Photonics for Biomedical Engineering. Netherlands: Springer; 2013. Lab-on-a-Chip Device and System for Point-of-Care Applications; p. 1-30.
44. Wu, Tsung-Feng, et al. An optical-coding method to measure particle distribution in microfluidic devices. AIP advances. 2011; 1.2:022155.
45. Mei, Zhe, et al. Applying an optical space-time coding method to enhance light scattering signals in microfluidic devices. Biomicrofluidics. 2011; 5.3:034116.
46. Deinard, Amos S., et al. Studies on the neutropenia of cancer chemotherapy. Cancer. 1974; 33.5:1210–1218. [PubMed: 4595975]

47. Crawford, Jeffrey, et al. Reduction by granulocyte colony-stimulating factor of fever and neutropenia induced by chemotherapy in patients with small-cell lung cancer. New England Journal of Medicine. 1991; 325.3:164–170. [PubMed: 1711156]
48. Martinez, Andres W., et al. Diagnostics for the developing world: microfluidic paper-based analytical devices. Analytical chemistry. 2009; 82.1:3–10. [PubMed: 20000334]
49. Mao, Xiaole; Huang, Tony Jun. Microfluidic diagnostics for the developing world. Lab on a Chip. 2012; 12.8:1412–1416. [PubMed: 22406768]
50. Martinez, Andres W., et al. Diagnostics for the developing world: microfluidic paper-based analytical devices. Analytical chemistry. 2009; 82.1:3–10. [PubMed: 20000334]
51. Yager, Paul, et al. Microfluidic diagnostic technologies for global public health. Nature. 2006; 442.7101:412–418. [PubMed: 16871209]
52. Klabunde, Thomas; Hessler, Gerhard. Drug design strategies for targeting G-protein-coupled receptors. Chembiochem. 2002; 3.10:928–944. [PubMed: 12362358]
53. Fredriksson, Robert, et al. The G-protein-coupled receptors in the human genome form five main families. Phylogenetic analysis, paralogon groups, and fingerprints. Molecular pharmacology. 2003; 63.6:1256–1272. [PubMed: 12761335]
54. Sullivan, Gary J.; Baker, Richard L. Efficient quadtree coding of images and video. Image Processing, IEEE Transactions on. 1994; 3.3:327–331.
55. Dransfield, Ian S.; Stocks, Craig; Haslett, C. Regulation of cell adhesion molecule expression and function associated with neutrophil apoptosis. Blood. 1995; 85.11:3264–3273. [PubMed: 7538822]
56. Arnal, Isabelle; Wade, Richard H. How does taxol stabilize microtubules? Current Biology. 1995; 5.8:900–908. [PubMed: 7583148]
57. Kim, Kyung Sook, et al. AFM-detected apoptotic changes in morphology and biophysical property caused by paclitaxel in Ishikawa and HeLa cells. PloS one. 2012; 7.1:e30066. [PubMed: 22272274]

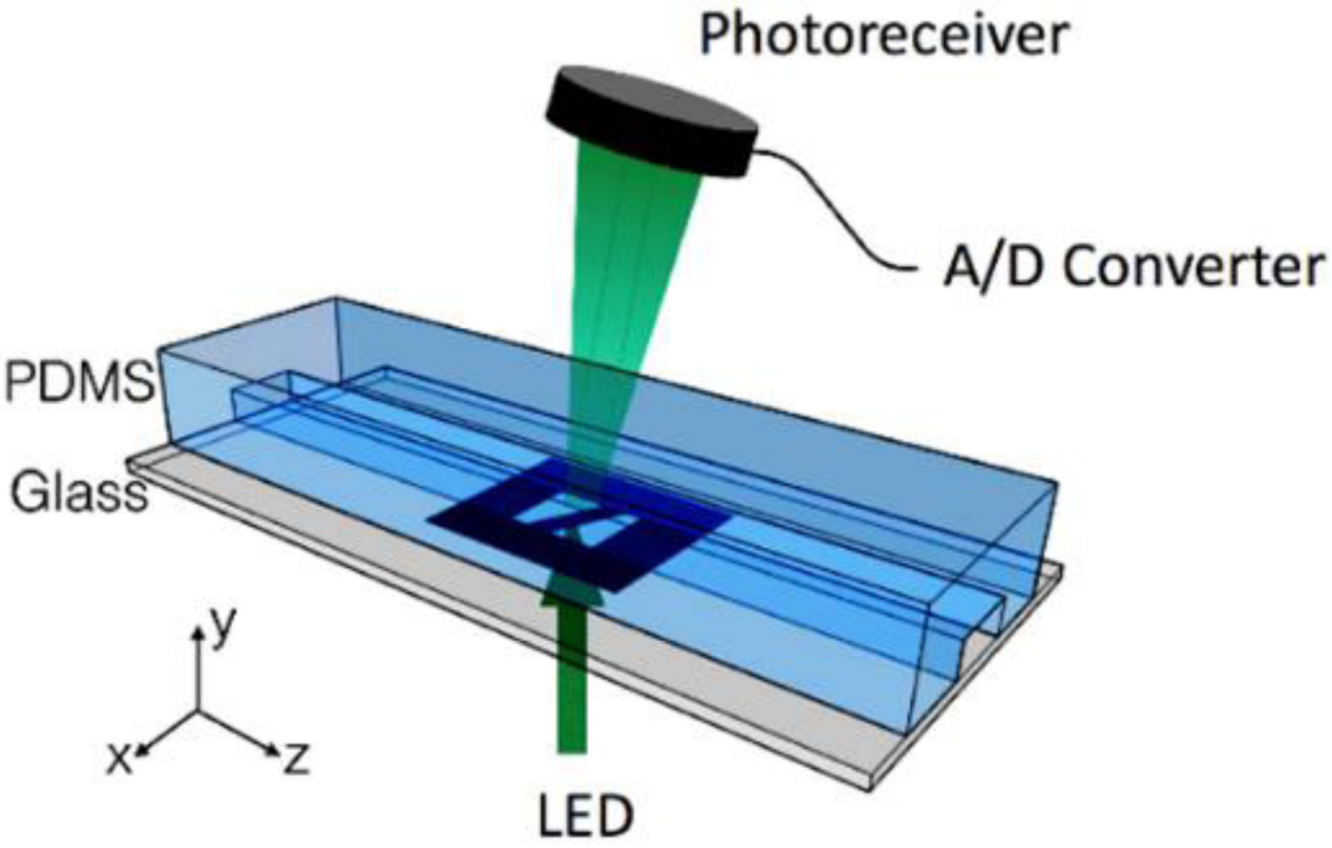

Fig. 1.
Experiment setup with space coding method

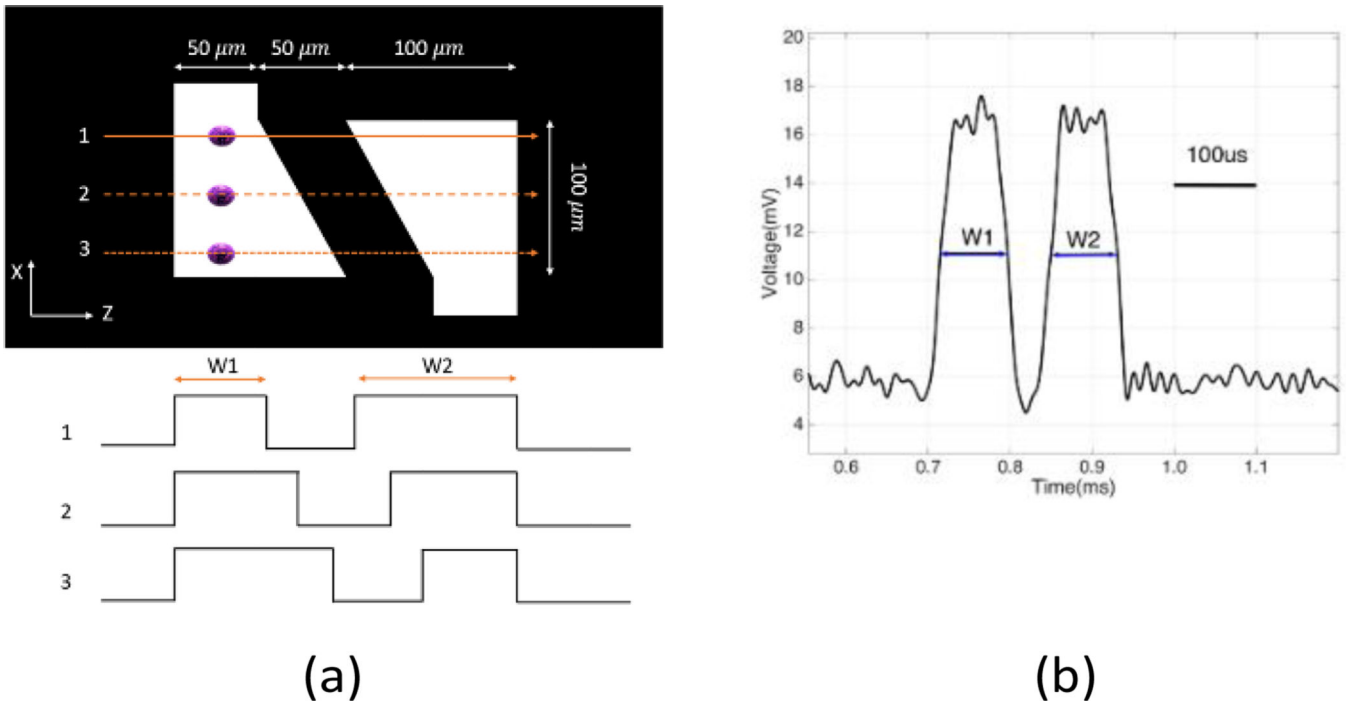

Fig. 2.

(a) Spatial mask design with two oppositely oriented trapezoidal slits. W1 and W2 represent the widths of the slits experienced by a cell traversing the mask from different positions. Also shown are the anticipated waveforms for cells crossing the mask area via different paths. (b) Intensity modulated forward scattering signal by the trapezoidal slits.

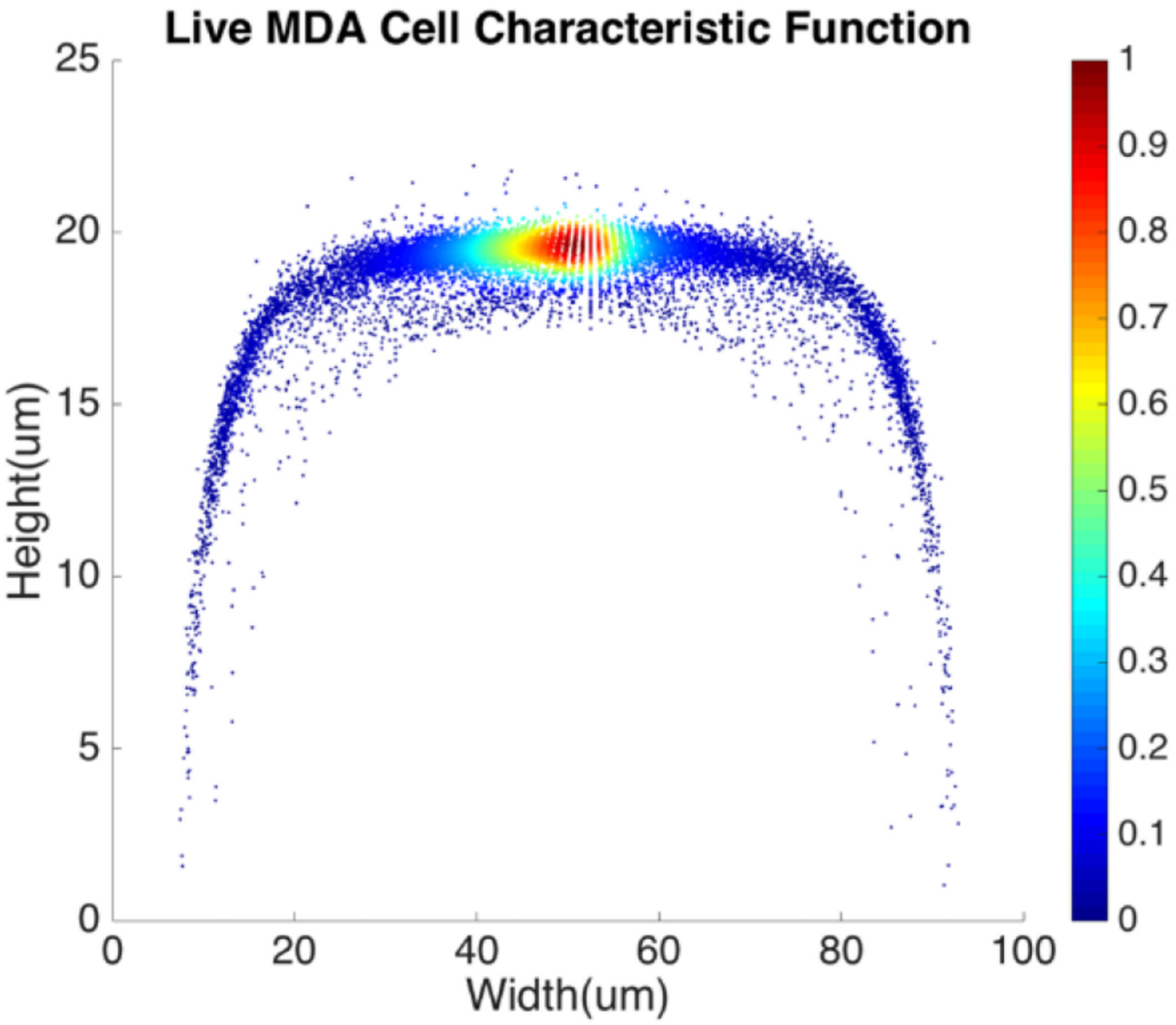

Fig. 3.
Spatial characteristic function of live MDA-MB-231 cell.

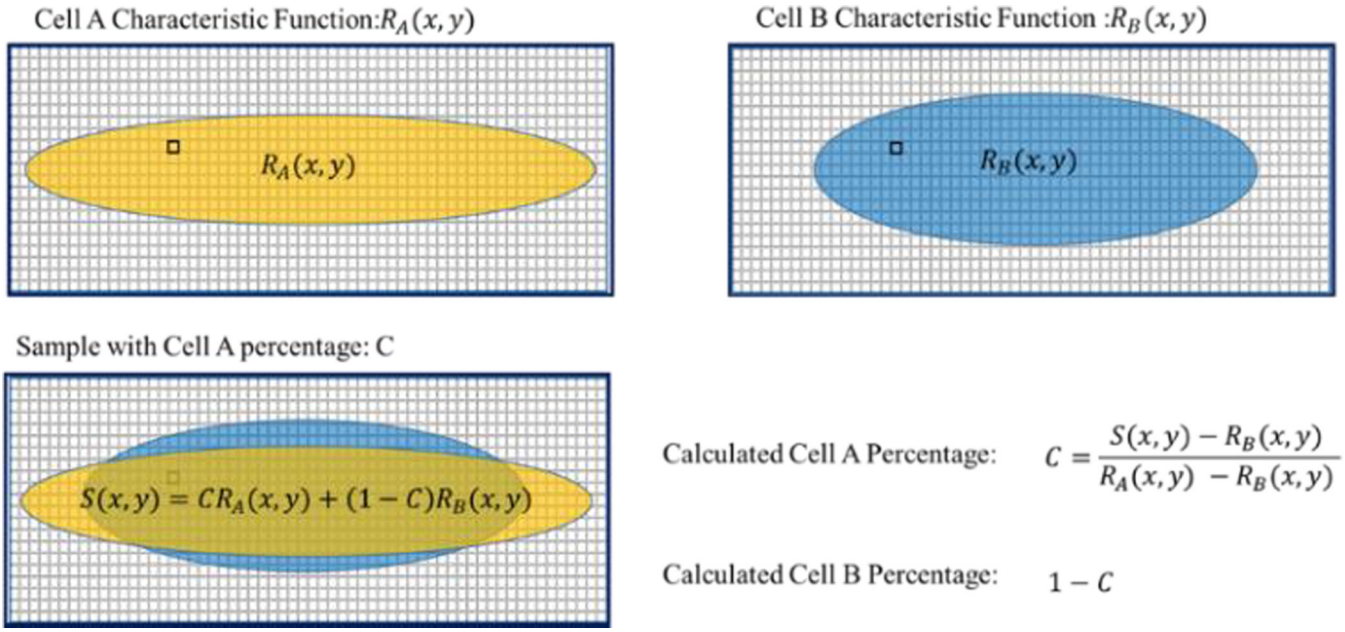

Fig. 4.

Illustration of the steps to calculate the cell ratio in a sample of cell mixture. The yellow and blue patterns represent the characteristic distributions for cell A and cell B.

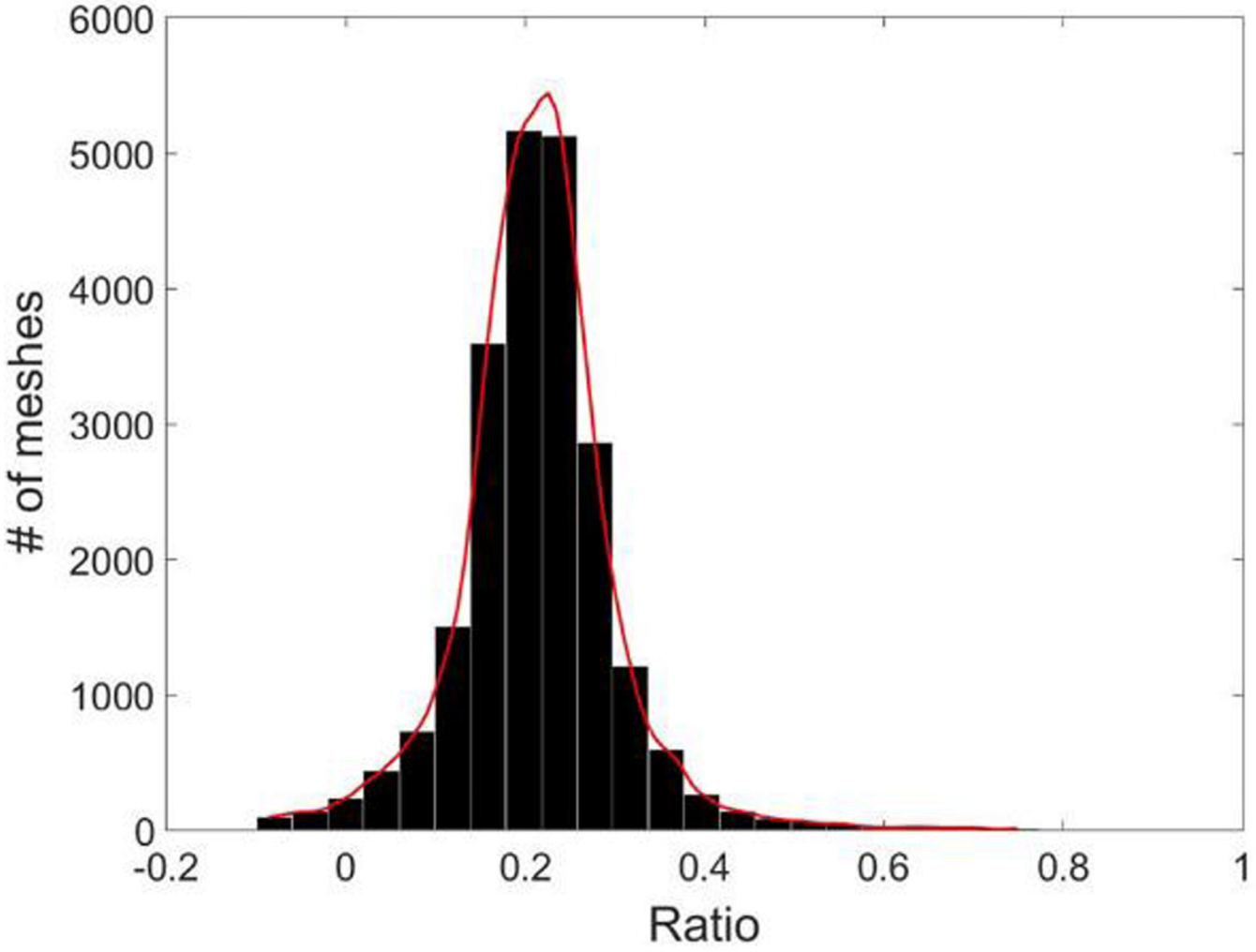

Fig. 5.
Histogram of the live MDA-MB-231 cell ratio, C.

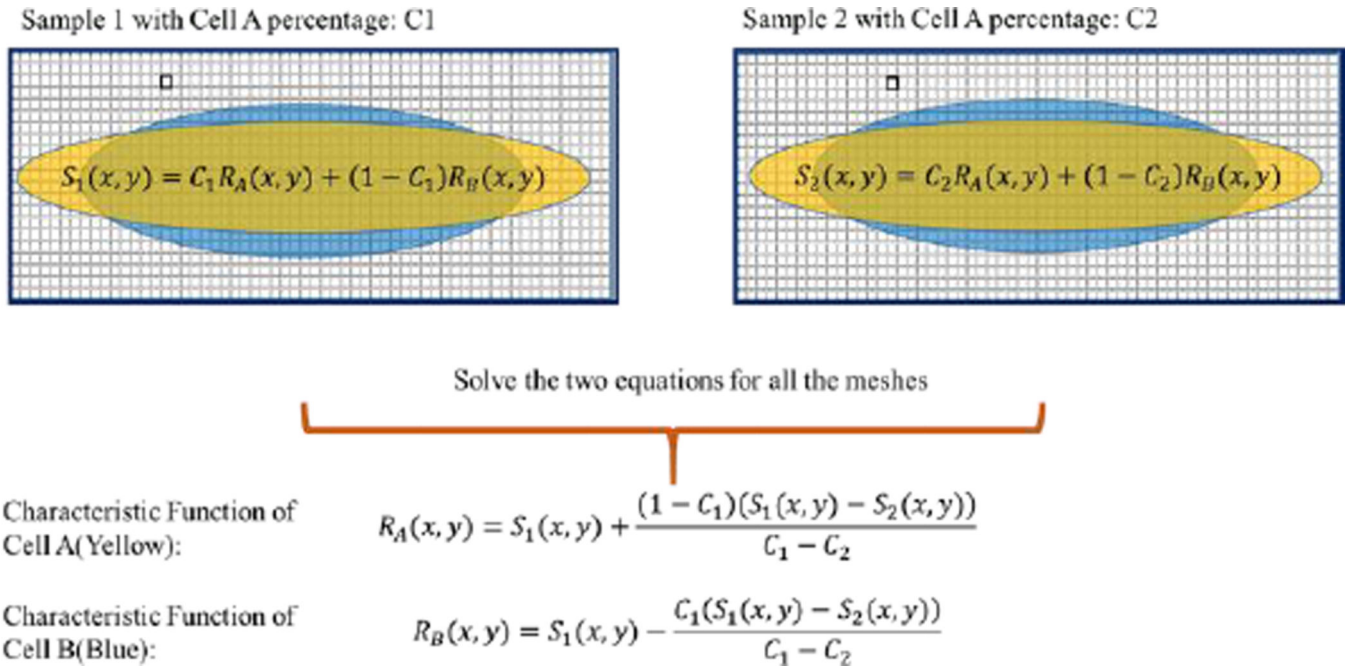

Fig. 6.
Use of cell mixtures as training samples to obtain the characteristic function of specific cell type.

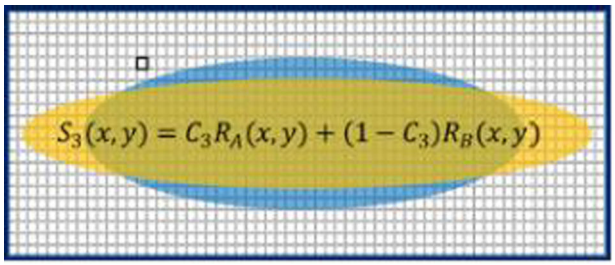

Calculated Cell A Percentage: $C_3 = \frac{S_3(x,y) - R_B(x,y)}{R_A(x,y) - R_B(x,y)}$

Calculated Cell B Percentage: $1 - C_3$

Fig. 7.
Test Sample Ratio calculation.

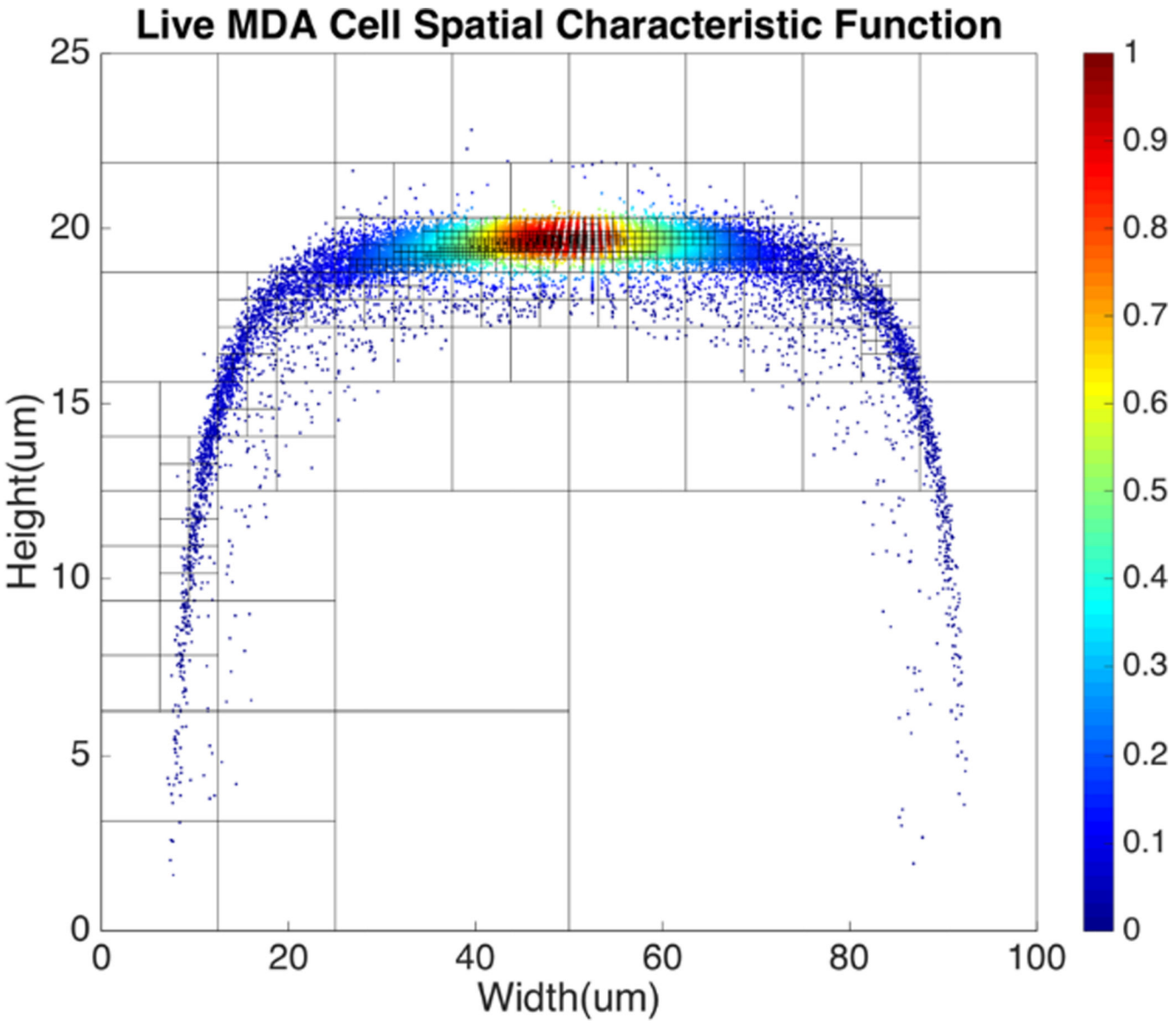

Fig. 8.

Spatial distribution of live MDA-MB-231 cells using meshes created by the quad-tree algorithm.

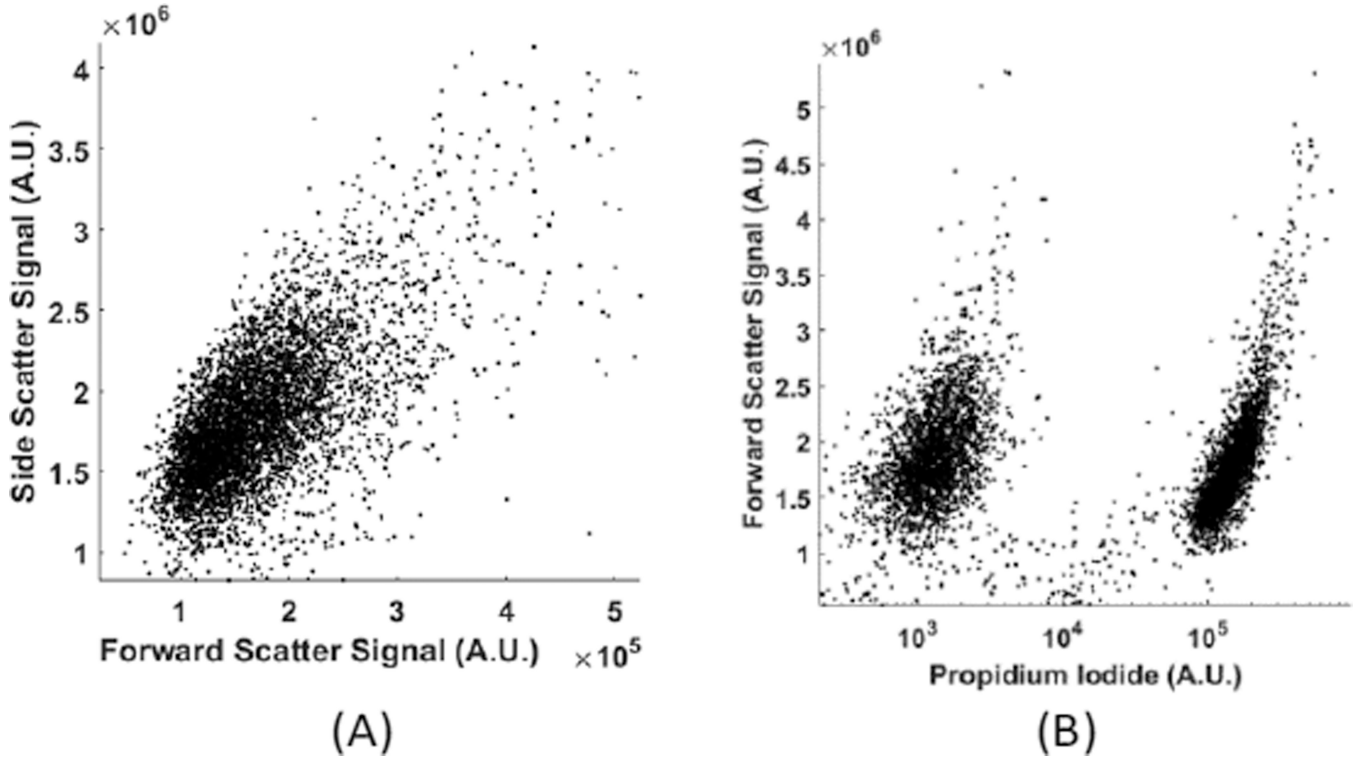

Fig. 9.

(A) Forward and side scattering of live and fixed MDA-MB-231 cells; (B) fluorescent signal of live and fixed MDA-MB-231 cells. The cluster on the left was auto fluorescence from live cells and the cluster on the right was Propidium Iodide labelled fluorescent signal from fixed cells.

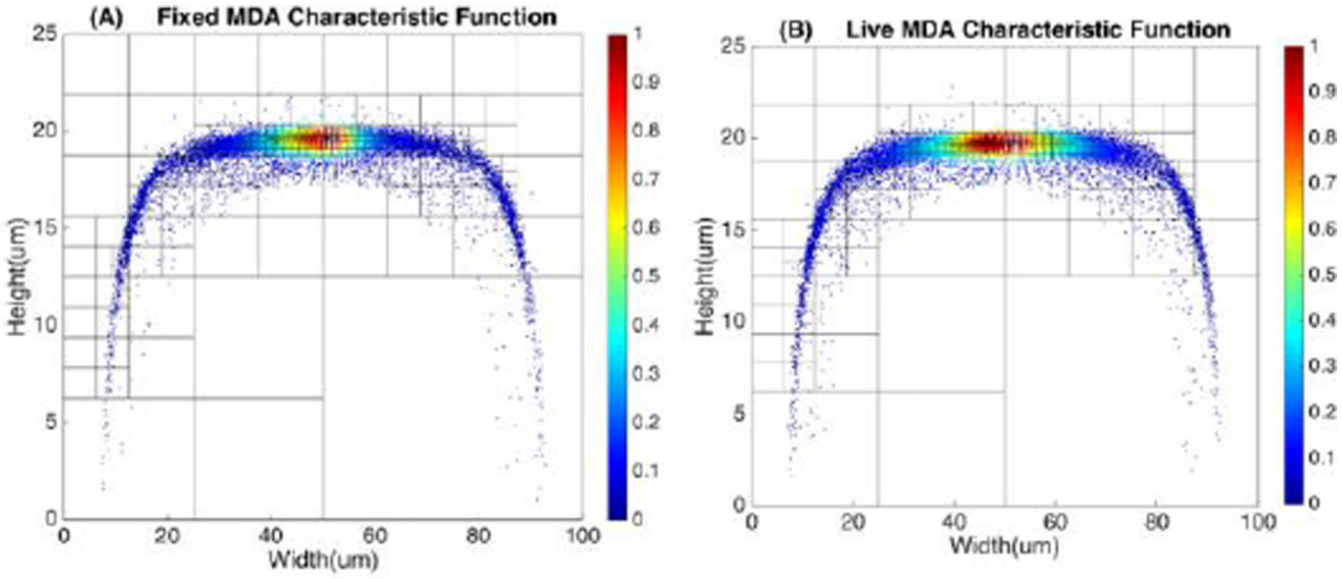

Fig. 10.
Characteristic function for fixed and live MDA-MB-231 cells.

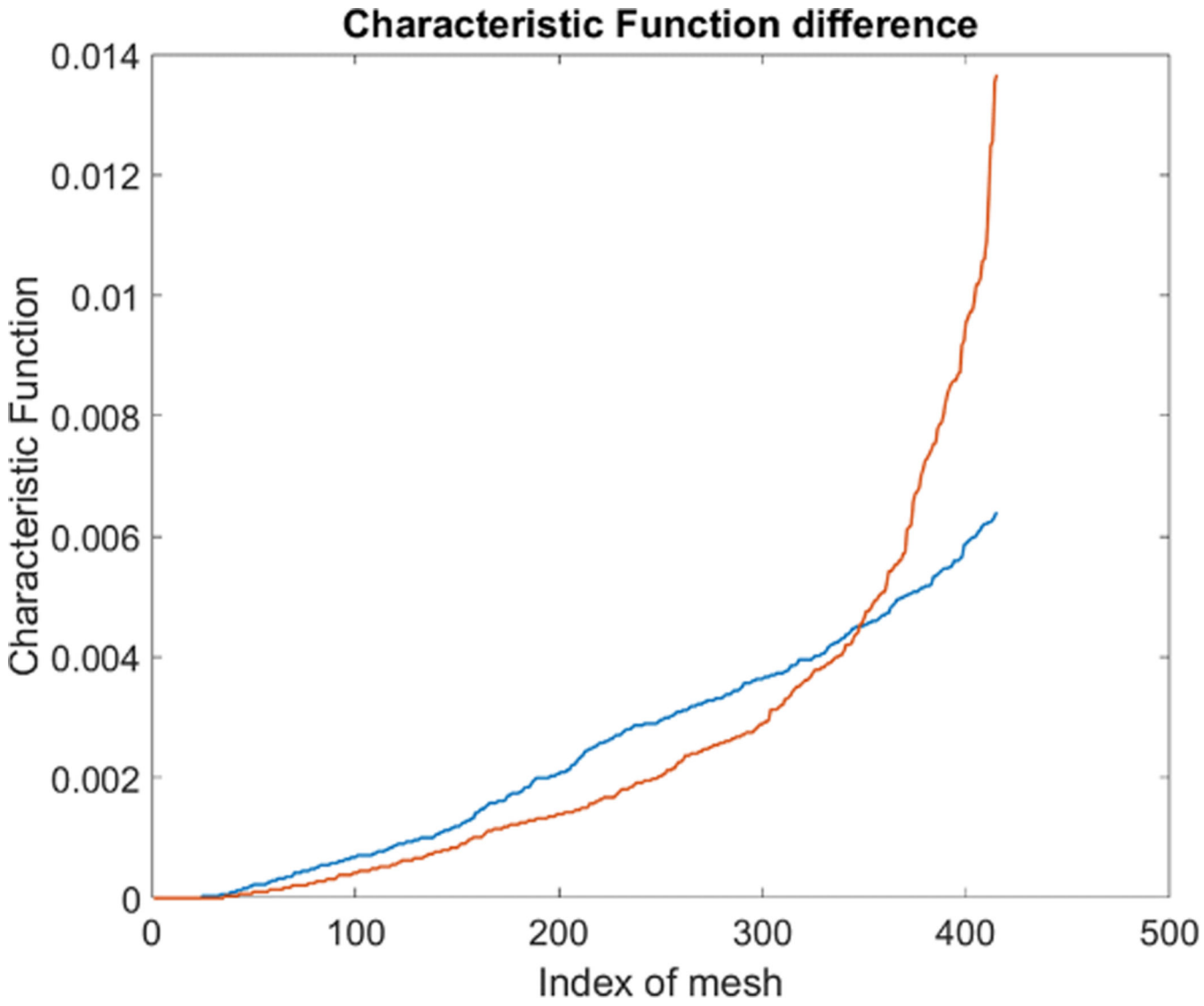

Fig. 11.

Characteristic function difference between live(Orange) and fixed(Blue) MDA-MB-231 cells. The steeper rise in the orange curve indicates that the live MDA cells are spatially more concentrated to certain ares in the channel than the fixed MDA cells.

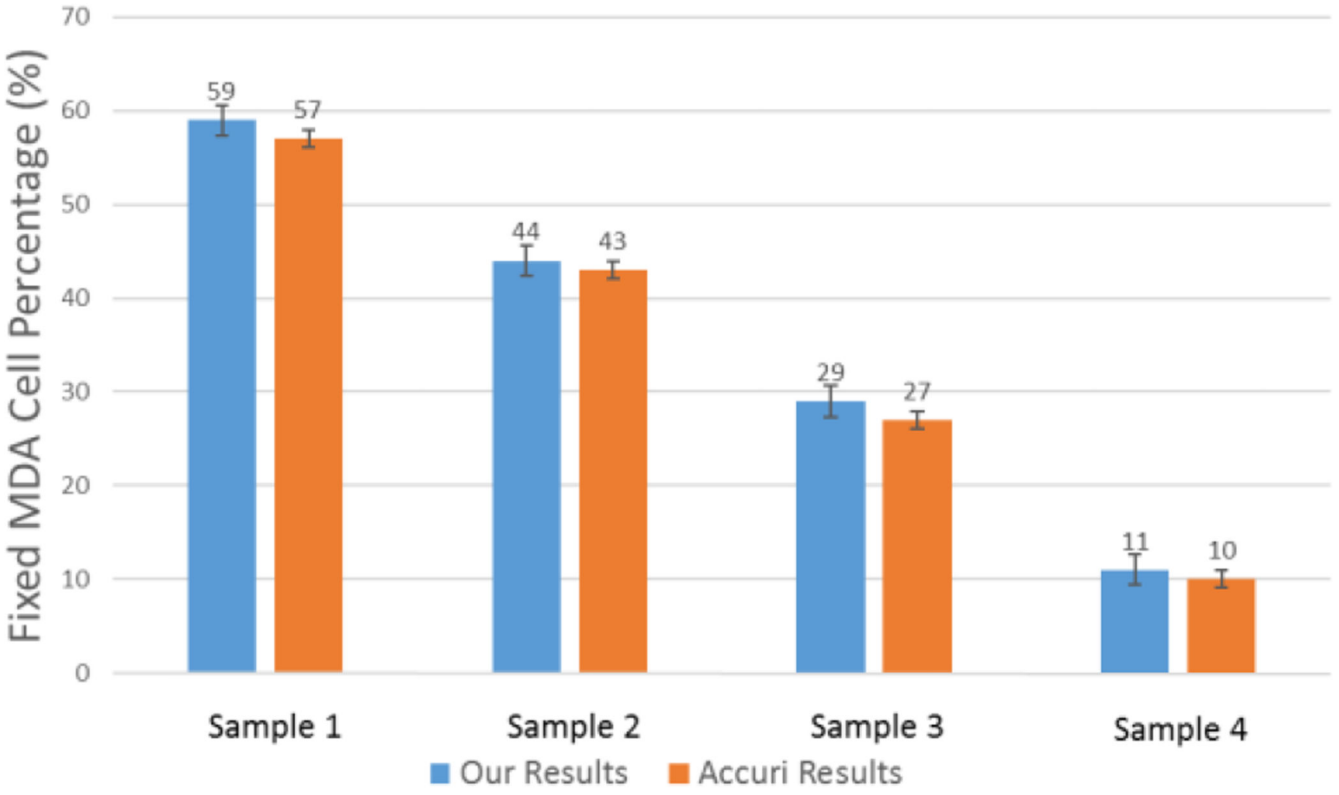

Fig. 12.

Measured mean value of live cell percentage in 4 samples. The error bars show the variations for 10 repeats for cytometer (Accuri C6).

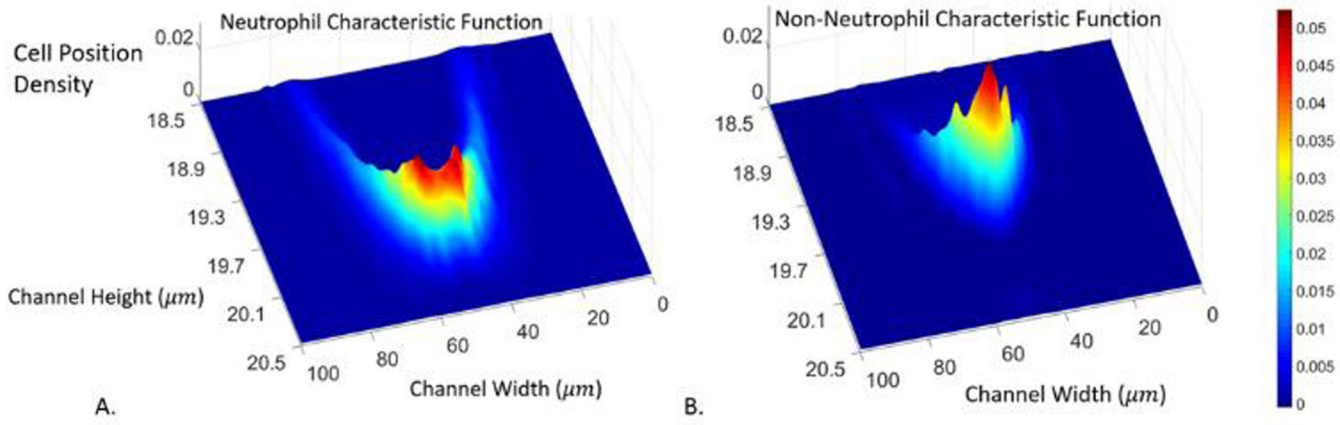

Fig. 13.
Neutrophil and Non-neutrophil characteristic functions.

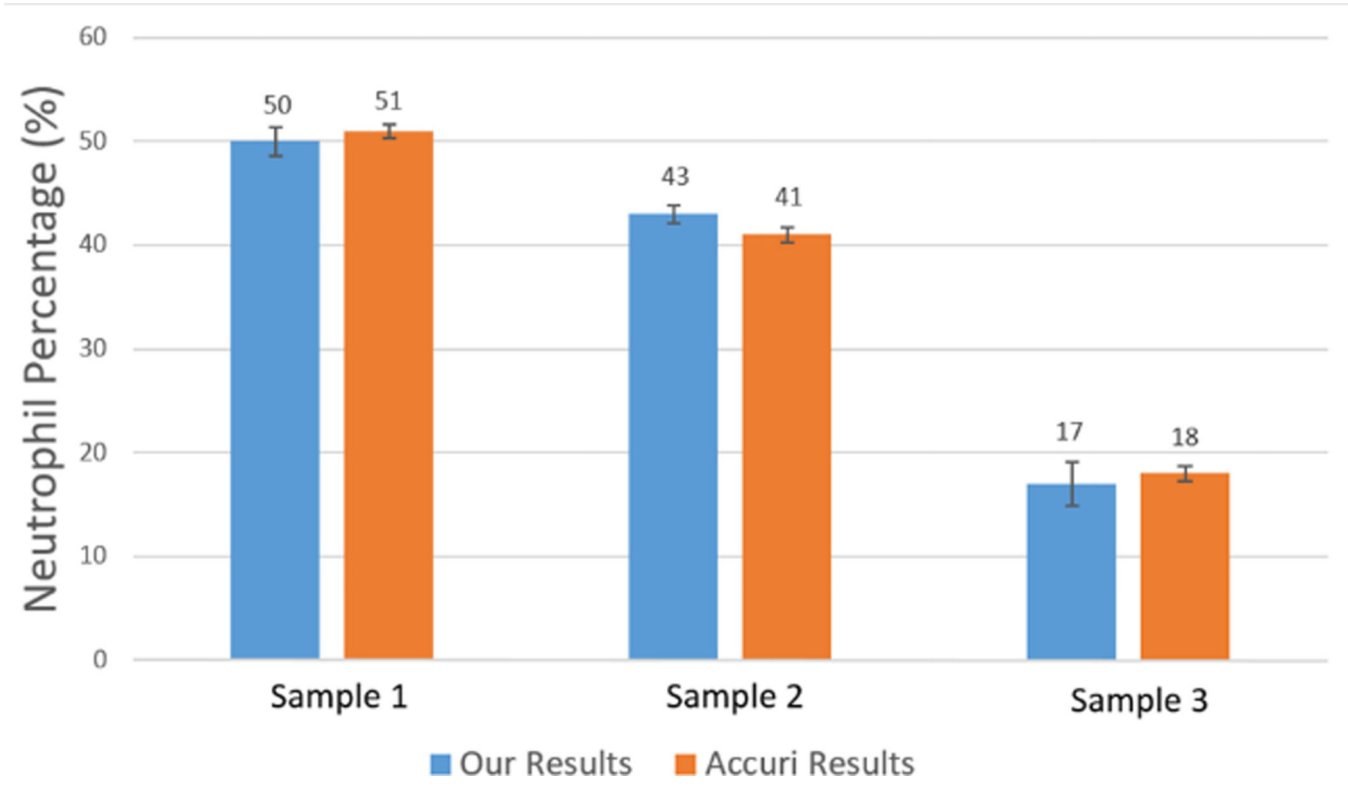

Fig. 14.

Measured mean value of neutrophil percentage over WBCs in 3 samples. The error bars show the variations for 10 repeats for each sample using our method and a commercial flow cytometer (Accuri C6).

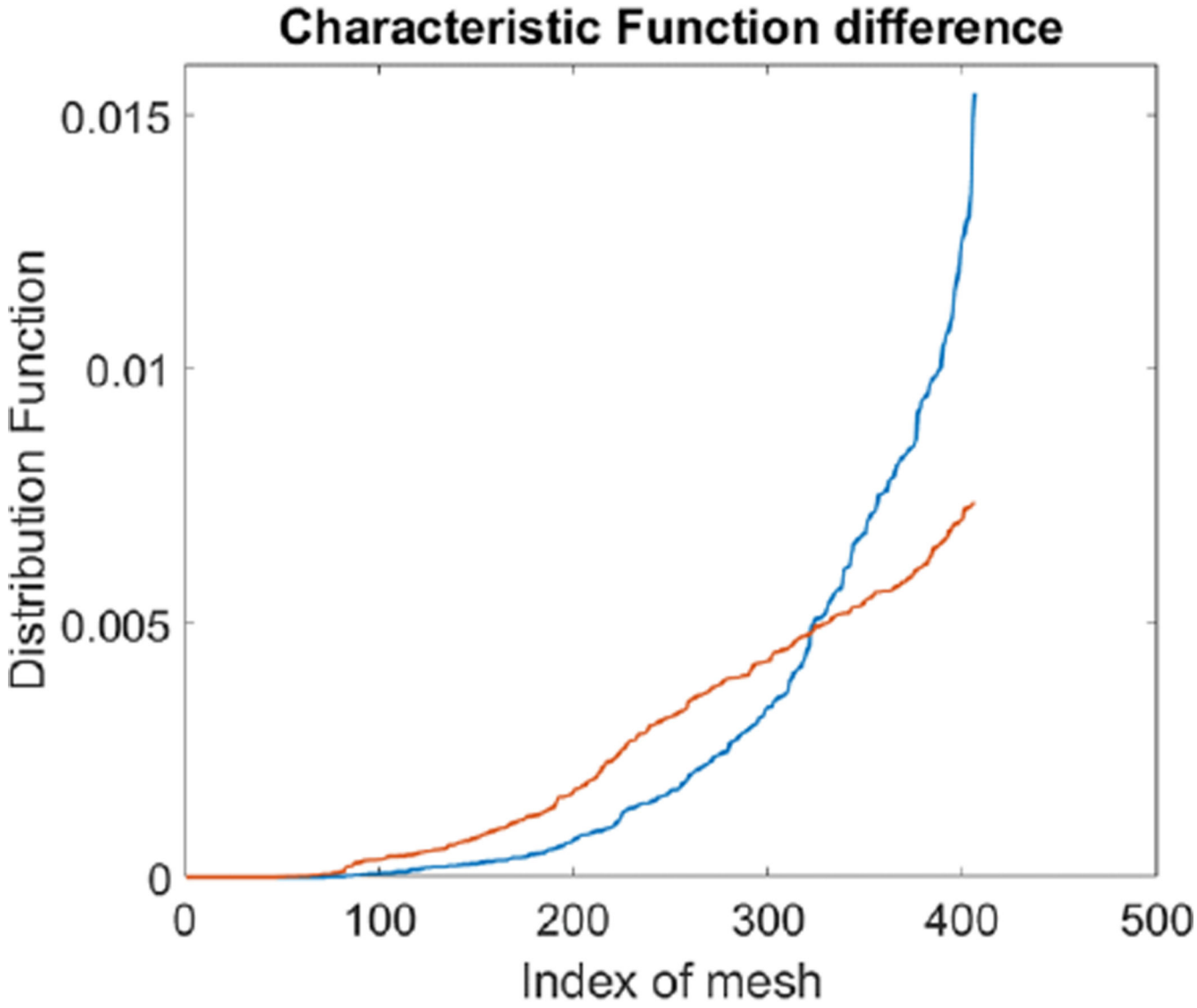

Fig. 15.

Difference in characteristic function for MDA-MB-231 cell with (Blue) and without (Orange) Paclitaxel treatment. The steeper rise in the blue curve indicates that the Paclitaxel treated cells are spatially more concentrated to certain ares in the channel than the untreated cells.

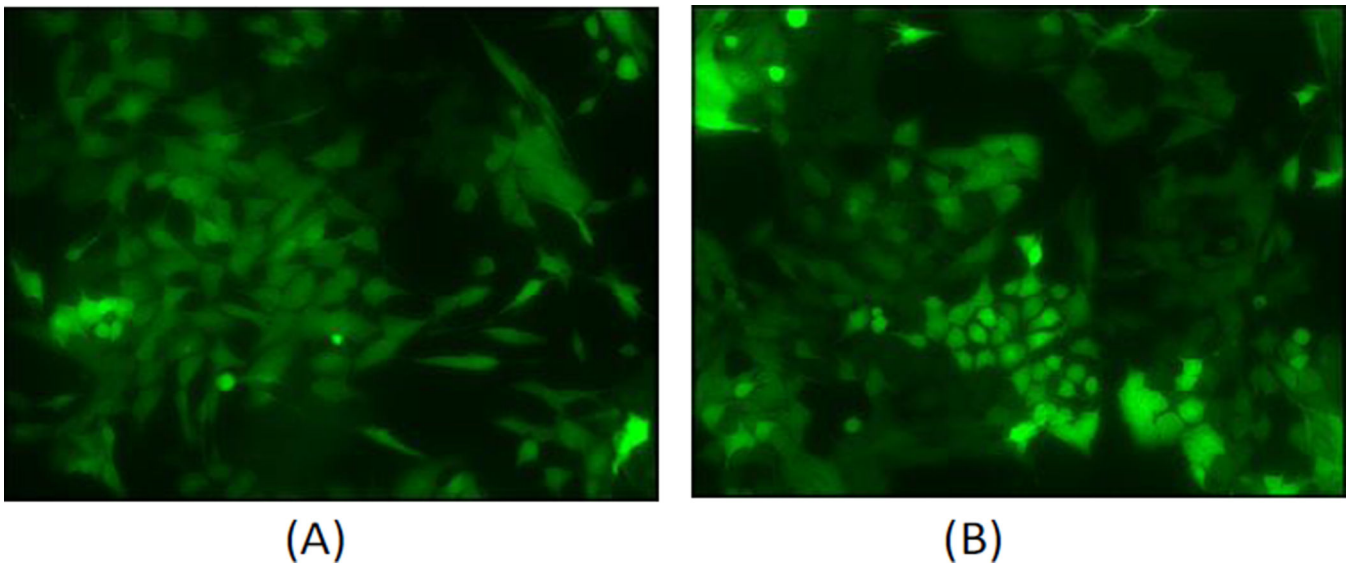

Fig. 16.

(A) is the fluorescent microscope picture of GFP transfected MDA-MB-231 cells without Paclitaxel treatment. (B) is fluorescent microscope picture of GFP transfected MDA-MB-231 cells with Paclitaxel treatment. It is difficult to tell the morphological differences using conventional histology.

Table 1

Measured neutrophil percentage over WBCs from 8 blood samples using our method and a commercial flow cytometer. Samples 9 and 10 were used to obtain the characteristic functions for neutrophil and non-neutrophil.

Test			
Sample	**Flowcytometer (%)**	**Our Methods (%)**	**Deviation (%)**
1	50	52	4.0
2	50	51	2.0
3	56	58	3.6
4	59	59	0.0
5	64	62	3.1
6	50	50	0.0
7	66	64	3.0
8	52	52	0.0
Training			
9	60		
10	49		